a reprint from Applied Optics

Optical constants of liquid and solid methane

John V. Martonchik and Glenn S. Orton

The optical constants $n_r + in_i$ of liquid methane and phase I solid methane were determined over the entire spectral range by the use of various data sources published in the literature. Kramers–Kronig analyses were performed on the absorption spectra of liquid methane at the boiling point (111 K) and the melting point (90 K) and on the absorption spectra of phase I solid methane at the melting point and at 30 K. Measurements of the static dielectric constant at these temperatures and refractive indices determined over limited spectral ranges were used as constraints in the analyses. Applications of methane optical properties to studies of outer solar system bodies are described.

Introduction

Methane in the gas phase has been observed in the atmospheres of the outer planets as well as some of their larger satellites. It is anticipated that methane in both the liquid phase and the solid phase also is present in the outer planets and satellites, either as a cloud layer or an aerosol haze in the upper atmosphere or as precipitation. When the results of theoretical modeling of such atmospheres are compared with spectral radiance observations taken either from Earth or spacecraft, information about the radiative structure and chemistry of the atmosphere can be deduced. It is important, however, that the modeling procedure has available the necessary input parameters to perform the required calculations accurately. In particular, to calculate the radiative effects of liquid and solid methane in planetary atmospheres, the corresponding optical constants, i.e., the refractive index n_r and the absorption index n_i, must be known as a function of wavelength.

At atmospheric pressure liquid methane exists near the triple point and thus has a limited temperature range, extending from approximately 90 to 111 K. Solid methane is known to exist in three phases for pressures below 1 kbar, but the thermodynamic conditions encountered in the atmospheres of the outer planets are such that only phase I solid methane (temperature >20 K at atmospheric pressure) will be present. This form has a face-centered cubic structure and therefore does not exhibit birefringence.

The results of a literature search for quantitative spectral information on the optical properties of methane in its condensed phases are presented. The data are then analyzed by means of the Kramers–Kronig dispersion relation and the resulting optical constants $n_r + in_i$ of the liquid and the phase I solid are displayed in tabular form.

Spectrum Features

Both the liquid phase and the solid phase I of methane have similar absorption spectra. The low-frequency end of the spectrum is characterized by a smooth, broad rotational–translational band centered at approximately 175 cm^{-1} and extending out to approximately 400 cm^{-1}. At higher frequencies, three strong, sharp fundamental vibrational bands are evident, ν_4 at 1300 cm^{-1}, ν_1 at 2820 cm^{-1}, and ν_3 at 3010 cm^{-1}. In the solid phase, combinations of fundamental and lattice vibrations also appear at 1350 and 3060 cm^{-1}. At the near-infrared and visible frequencies the liquid-phase spectrum is characterized by many weak vibrational overtone bands that correlate well with the corresponding gas absorptions but are shifted toward the lower frequencies by 35–50 cm^{-1} and are generally wider in nature.[1] In the far ultraviolet a strong absorption continuum appears at approximately 74 000 cm^{-1} (135 nm) because of molecular electronic transitions.

Condensed Methane Absorption Data Sources

Liquid Phase

Savoie and Fournier[2] (SF) obtained a far-infrared transmission spectrum of a 2-mm sample of liquid

The authors are with the Jet Propulsion Laboratory, California Institute of Technology, 4800 Oak Grove Drive, Pasadena, California 91109.

Received 13 May 1994; revised manuscript received 15 July 1994.
0003-6935/94/368306-12$06.00/0.

methane at 98 K in a study of lattice symmetry of tetrahedral molecules. The data were recorded at a spectral resolution of 1 cm^{-1} and covered the region 20–200 cm^{-1}.

Arning, Tibulski, and Dorfmuller[3] (ATD) obtained far-infrared spectra of liquid alkanes, including methane at 100 K, in a study of relaxation times and molecular motion. The data are graphically displayed as Lambert absorption coefficients that cover the frequency range 15–275 cm^{-1}.

Weiss, Leroi, and Cole[4] (WLC) show a transmission spectrum of methane at 100 K that covers the frequency range 200–500 cm^{-1}. The spectral resolution was 1.5–2 cm^{-1}, and the sample had a thickness of 2.5 mm. This was part of a study of the infrared octupole-induced spectrum of methane gas at room temperature.

Pinkley, Sethna, and Williams[5] (PSW) obtained spectral reflectance measurements of methane at 98 K that covered the frequency range 400–4000 cm^{-1}. Results are presented as optical constants in both graphical and tabular form.

Ramaprasad, Caldwell, and McClure[6] (RCM) present transmission spectra recorded on photographic plates of a 3-cm-thick liquid methane sample at 91–99 K. The data include the bands in the frequency range 5155–16 155 cm^{-1} (619–1940 nm).

Patel, Nelson, and Kerl[1] (PNK) show an uncalibrated absorption spectrum of liquid methane at 94 K, obtained with an opto-acoustic technique and covering the frequency range 13 300–18 100 cm^{-1} (550–750 nm).

Solid Phase

SF obtained a far-infrared transmission spectrum of solid methane at 77 K (phase I) for the same instrumental conditions as liquid methane. Also obtained was a spectrum of a solid sample in phase II at 12 K.

Obriot, Fondere, Marteau, Vu, and Kobashi[7] (OFMVK) presented a transmission spectrum of a 2-mm-thick methane sample at 30 K (phase I) that covered a frequency range 30–250 cm^{-1}. This was part of a study of solid methane under high pressure.

Fink and Sill[8] (FS) obtained spectra of methane at 52 K (phase I) as part of a study of the absorption properties of condensed volatiles in the outer solar system. An interferometer that covered the frequency range 1200–4000 cm^{-1} and had a resolution of better than 1 cm^{-1} was used. A variety of different sample thicknesses were used, all in the micrometer range, and the results were tabulated as absorption coefficients.

Roux, Wood, Smith, and Plyler[9] (RWSP) obtained transmission spectra of methane at 20 K (probably phase I) in an investigation to assess the degradation of cryogenically cooled optical surfaces contaminated by condensed gases. They used an interferometer at 4-cm^{-1} resolution that covered the frequency range 500–3700 cm^{-1}. Data were collected for 24 sample thicknesses ranging from 0.242 to 11.35 μm, and the results were tabulated as optical constants.

Khare *et al.*[10] and Pearl, Ngoh, Ospina, and Khanna[11] (PNOK) made transmission measurements for a number of thin-film samples (thicknesses between 1.2 and 215μm) of phase I and phase II methane at 30 and 10 K, respectively, in an ongoing study of the optical properties of materials of planetary interest. Khare *et al.* listed absorption indices for phase I methane between 3800 and 9000 cm^{-1} (1.12–2.63 μm), and PNOK determined optical constants for both phase I and phase II methane between 1200 and 9000 cm^{-1}.

Dressler and Schnepp[12] obtained ultraviolet transmission spectra of methane at 4.2 K (phase II or possibly phase III) during a study of intermolecular interactions in hydride molecules. The spectra cover the frequency range 70 000–86 000 cm^{-1} (110–130 nm) and were obtained for a variety of film thicknesses between 0.01 and 30 μm. The data were displayed graphically as molar absorption coefficients.

In addition to these absorption data, measurements of the static dielectric constant and related parameters were made by Costantino and Daniels[13] for solid methane at a variety of pressures and temperatures. Amey and Cole[14] also measured the dielectric constant for both liquid and solid methane near the melting point and for liquid methane at the boiling point. These data are useful in constraining the refractive-index spectrum, derived from the absorption data by the use of a Kramers–Kronig analysis, as described below.

Analysis

The Kramers–Kronig dispersion relation can be written as

$$n_r(\sigma) = 1 + \frac{2}{\pi} P \int_0^\infty \frac{n_i(\sigma')\sigma' d\sigma'}{\sigma'^2 - \sigma^2}, \quad (1)$$

where $n_r(\sigma)$ is the refractive index at frequency σ, $n_i(\sigma)$ is the absorption index at σ, and P implies the Cauchy principal part of the integral. The absorption index, in turn, can be obtained from the transmission $T(\sigma)$ through a sample of thickness d,

$$T(\sigma) = \exp[-a(\sigma)d], \quad (2)$$

where $a(\sigma) = 4\pi\sigma n_i(\sigma)$ is the absorption coefficient at σ. In an application of Eq. (1), Martonchik *et al.*[15] determined the index of refraction of ammonia ice from the ultraviolet to the far infrared by the use of the spectral absorption data found in the literature. If information about the absorption-index spectrum is missing in regions where significant absorption occurs, direct application of Eq. (1) can result in an underestimate of $n_r(\sigma)$ at most frequencies. The absorption data for both solid and liquid methane are fairly complete, except in the wavelength region shortward of the blue. Therefore it is desirable to have some knowledge of the refractive index at one or

more frequencies to serve as constraints on the integration process described by Eq. (1).

For nonpolar molecules, the refractive index at zero frequency, $n_r(0)$, is directly related to the static dielectric constant ε_s by the Maxwell relation $\varepsilon_s = n_r(0)^2$. Amey and Cole[14] measured the static dielectric constant of liquid methane near the melting point (90 K) and the boiling point (111 K). The resulting refractive indices $n_r(0)$ are 1.293 and 1.274, respectively, with an uncertainty of approximately 0.0005. For temperatures between the melting and boiling points, Amey and Cole found that the corresponding $n_r(0)$ could be accurately determined by the use of linear interpolation.

Additional liquid-methane refractive indices in the visible region of the spectrum were determined by Arakawa *et al.*[16] with an ellipsometric technique in a study of the optical properties of materials of planetary interest. For a temperature of approximately 111 K, they obtained a number of n_r values between wavelengths 0.4 and 2.0 μm, ranging from 1.278 at 2.0 μm to 1.286 at 0.4 μm, with a listed uncertainty of approximately 0.005.

The Costantino and Daniels[13] expression for ε_s of solid methane, based on laboratory experiments, depends both on density and temperature. Although their results were obtained for pressures greater than 3 kbars and temperatures ranging from 70 to 240 K, extrapolation to a pressure of 1 bar produced results in excellent agreement with the measurements of Amey and Cole,[14] the only other source of ε_s data known to us. Amey and Cole measured the static dielectric constant of solid methane near the melting point (90 K), implying a value of $n_r(0)$ equal to 1.319 ± 0.0005; the extrapolated value deduced from the Costantino and Daniels data is 1.320 ± 0.003, assuming a density of 0.492 gm cm^{-3}. The Costantino and Daniels data also show a linear relationship between ε_s and temperature for a given pressure, with the slope independent of pressure. Assuming that this relationship is also valid at 1 bar, we can infer that $n_r(0)$ at 70 K is 1.320 ± 0.0005. Extrapolating the temperature down to 20 K implies that $n_r(0)$ is 1.322 ± 0.001, with a corresponding density of 0.493 ± 0.010 gm cm^{-3}. Measurements[17] near this temperature, however, indicate a density greater than 0.52 gm cm^{-3} that, if true, would appear to invalidate extrapolation to temperatures this low.

A determination of the refractive index for solid methane at a temperature of 33 K was made by Khare *et al.*[10] with a dual-angle laser interference technique. They found a value of 1.302 ± 0.002 at a wavelength of 633 nm, in agreement with a less accurate value of 1.31 ± 0.02, which they also determined with a different interference-measurement technique. Another refractive-index determination for solid methane at a temperature of 20 K and the same wavelength of 633 nm was made by RWSP, but the value of 1.35 ± 0.03 that they found does not have an accuracy as high as those of Khare *et al.* RWSP also deduced that the density of their sample was 0.426 gm cm^{-3}, which is significantly lower than the value of 0.50–0.53 gm cm^{-3} at 20 K found by other investigators.[17] This may imply that the RWSP sample, a thin-film deposition, is not representative of bulk solid methane.

Absorption-Index Spectrum of Liquid Methane

0–500-cm^{-1} Spectral Region

The absorption indices obtained from the spectral data of SF,[2] ATD,[3] and WLC,[4] are shown in Fig. 1, which illustrates considerable differences between the three data sets. Both the SF and the WLC sets were originally expressed in terms of transmission, and no quantitative analysis was directly performed on the spectra in either publication. Thus apparently no effort was made to correct the measured transmissions for any residual cell window effects to obtain accurate absorption indices. The ATD data, however, were originally presented as absorption coefficients, and the spectrum was subsequently analyzed to determine a correlation function. We therefore believe that the ATD data set is more accurate than the SF and WLC sets, and only the ATD data set was considered in the spectral range 0–300 cm^{-1}. For frequencies higher than 300 cm^{-1} the spectral trend illustrated in the WLC data was assumed, and the results were scaled to the ATD value at 300 cm^{-1}. In our analysis we estimated the uncertainty to be 10% for the value of the absorption indices at frequencies below 300 cm^{-1} and 20% at frequencies greater than 300 cm^{-1}.

500–4000-cm^{-1} Spectral Region

The only liquid-methane spectral data known to us in this region are those of PSW.[5] Their results for the absorption index are shown in Fig. 2. It can be seen from Fig. 2 that considerable background absorption exists in the data in addition to the fundamental vibration–rotation bands centered at 1300 and 3000 cm^{-1}. This background absorption is considerably

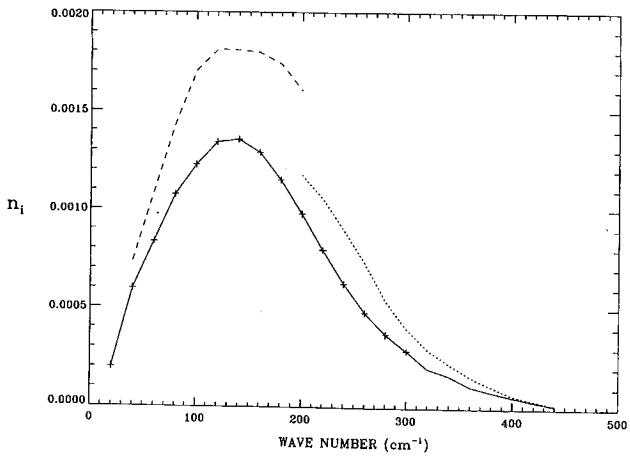

Fig. 1. Absorption-index spectra of liquid methane: Dashed curve, SF; dotted curve, WCL; crosses, ATD; solid curve, best estimate.

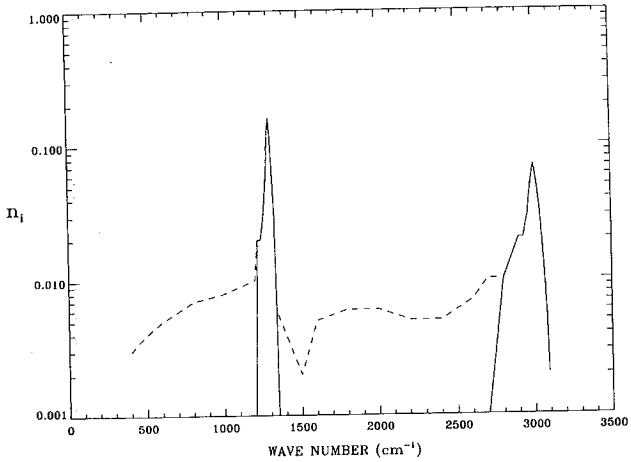

Fig. 2. Absorption-index spectra of liquid methane: Dashed curve, PSW; solid curve, best estimate.

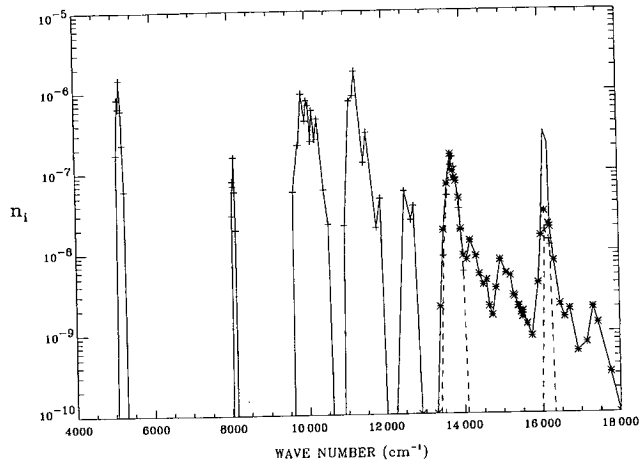

Fig. 3. Absorption-index spectra of liquid methane: Crosses, dashed curve, RCM; asterisks, PNK; solid curve, best estimate.

larger than the quoted uncertainties of the data, but the possible origin of the absorption was not discussed. Because comparable absorptions are not found in either the gas or the solid-phase spectrum, we believe that the background absorption is not real and is probably an artifact of the reflectance data analysis. Therefore we arbitrarily limited the absorption to the region between 1200 and 1350 cm^{-1}, which contains the ν_4 transition, and also to the region between 2850 and 3120 cm^{-1}, which contains the ν_1 and ν_3 transitions. This latter region in the PSW data is structurally unresolved compared with the same region in the solid-phase spectrum and may be the result of gaseous methane contamination of the reflectance measurements. We have not done any further reanalysis of the PSW data and have used the absorption indices as published except for the modifications described above. We believe, however, that this spectral region should be studied further to verify these results. An estimated uncertainty of 25% in the value of the absorption indices was assumed in the subsequent analysis.

5000–18 100-cm^{-1} Spectral Region

There are only weak absorption features in this part of the methane spectrum, but RCM and PNK have managed to obtain absorption data with spectral coverage of the two data sets that overlap near 13 700 cm^{-1}. The resulting absorption indices are illustrated in Fig. 3. Because the PNK opto-acoustic data are only relative measurements of absorption they were scaled to the RCM data at 13 700 cm^{-1}, the strongest absorption feature common to both data sets. The PNK data also are of higher quality than the RCM data, and in the region of overlap they were preferentially used in our analysis. The uncertainty in the resulting absorption indices was estimated to be 25%.

Frequencies Greater than 18 100 cm^{-1}

We could find no absorption measurements of liquid methane in this spectral region, but some data on the gaseous phase do exist. Khare *et al.*[10] has shown that in the red and the near-infrared parts of the spectrum the absorption indices of gaseous methane at low resolution are very similar to the those for the liquid phase, provided that the gas density is raised to the density of the liquid. A similar conclusion was reached by Pinkley *et al.*[5] for the fundamental bands. Therefore we present the gaseous data in this spectral range to complete our study of the characteristic features of the methane spectrum and also to use these data, appropriately scaled to the density of the liquid state, in our determination of spectral refractive indices.

A review of all the absorption cross-section measurements of methane gas from 2 to 160 nm (62 500 to 500 000 cm^{-1}) was completed by Hudson[18] in 1971; since then additional measurements in the wavelength range 140 to 160 nm were made by Mount *et al.*[19] We assume that the methane has a gas density at STP of 7.15×10^{-4} gm cm^{-3}, and the resulting absorption indices are illustrated in Fig. 4. Also shown in Fig. 4 are the scaled absorption indices for

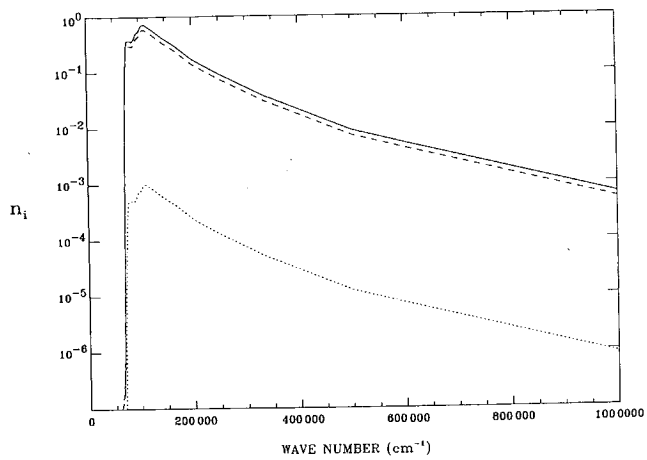

Fig. 4. Absorption-index spectra of methane: Dashed curve, liquid-phase best estimate; solid curve, solid-phase best estimate; dotted curve, gas phase.

the liquid phase, assuming a liquid-methane density of 0.424 g cm^{-3} (111 K). It is expected that the uncertainty in the indices will be large; we have assumed that the uncertainty is 50% for any given frequency. But it should be noted that the frequency-integrated absorption index is more tightly constrained because this spectral region dominates the integral described by Eq. (1) and the refractive index at zero frequency is well known.

Optical Constants of Liquid Methane

The use of the Kramers–Kronig relation in Eq. (1) with the absorption indices described above produced a refractive-index spectrum at the boiling point (111 K) that was close to, but consistently below, the measured indices of Arakawa *et al.*[16] and the value at zero frequency inferred from the static dielectric constant. A sample of the measured values of n_r and the corresponding computed values is listed in Table 1, which shows a difference maximum of approximately 0.018 at 1.0 and 2.0 μm and a difference minimum of 0.006 at zero frequency. Because the general level of the refractive indices throughout the spectrum is determined mainly by the absorption shortward of the ultraviolet wavelengths, this reasonably good agreement indicates that the scaled gaseous absorption values used in this spectral region are probably a fair representative of the actual liquid-methane spectrum.

In an effort to produce a better match between computations and measurements, we subsequently rescaled the gaseous absorption values by small amounts. An adjustment to this particular part of the liquid-methane absorption spectrum is reasonable because the original scaling factor, defined by the ratio of liquid density to gas density can only be considered an approximation. The rescaling results, also shown in Table 1, are for the two cases in which the absorption indices in Fig. 4 were increased by 2.5 and 5.7%. The smaller increase of 2.5% produces a refractive index at zero frequency, $n_r(0)$, that agrees with the static dielectric constant measured by Amey and Cole[14] but also produces indices in the visible and the near infrared that are consistently below the measurements of Arakawa *et al.* by approximately 0.011. The larger scaling increase of 5.7% results in refractive indices that are in good agreement with the Arakawa *et al.* values (all are within the 0.005 uncertainty) but overshoots $n_r(0)$ by 0.008. Other regions of the absorption spectrum are not strong enough for any reasonable resizing of their values (within the allowable uncertainty limits) to change the results in Table 1 significantly. For instance, if the collision-induced absorption region in the far infrared (Fig. 1) or the strongly absorbing fundamental bands between 1200 and 3100 cm^{-1} are scaled down by 50%, $n_r(0)$ is reduced by only 0.001 and 0.002, respectively. If we assume that the refractive indices of Arakawa *et al.* are correct, then the corresponding result of 1.282 for $n_r(0)$ implies a static dielectric of 1.644. This is larger than the value of 1.623 that was measured by Amey and Cole (and outside the uncertainty of 0.0005) and appears inconsistent with $n_r(0)$ determined at other temperatures, as discussed below.

Table 2 lists both refractive and absorption indices of liquid methane at both 111 and 90 K for selected frequencies. Those optical constants followed by a positive or negative sign indicate a local maximum or minimum, respectively. The refractive indices at 111 K were computed with the assumption that $n_r(0)$ is 1.274; this implies a rescaling of the far-ultraviolet absorption spectra shown in Fig. 4 by 2.5% and assumes that the rest of the absorption indices n_i are as indicated in Figs. 1–3. Using the static dielectric constant at 90 K of 1.672, as determined by Amey and Cole,[14] we assumed a value of 1.293 for $n_r(0)$ at the melting point. The n_i at 90 K were determined by simply scaling the n_i at 111 K by the ratio of the methane densities at these two temperatures. Because the uncertainties in the absorption indices are much larger than this first-order temperature correction, this temperature correction of n_i serves only to indicate the magnitude of the temperature dependence. The far-ultraviolet absorption indices then were scaled up by an additional 2.5% to achieve the assumed value of $n_r(0)$.

The region with frequencies greater than 60 000 cm^{-1} (167 nm) is also included in Table 2. Caution must be used, however, with regard to the optical constants listed for this spectral region, because they are based on an extrapolation from the gaseous phase. We believe, nevertheless, that these values represent a reasonable approximation to the actual optical constants.

Table 1. Liquid CH_4 Refractive Indices

Frequency (cm^{-1})	n_r[a]	n_r[b]	n_r[c]	n_r[d]	Wavelength (μm)
0	1.274	1.268	1.274	1.282	∞
5000	1.278	1.260	1.267	1.275	2.0
8333	1.280	1.262	1.268	1.277	1.2
10 000	1.280	1.262	1.269	1.277	1.0
12 500	1.281	1.264	1.270	1.279	0.8
16 667	1.283	1.266	1.273	1.282	0.6
25 000	1.286	1.273	1.281	1.289	0.4

[a] $n_r(0)$ determined by Amey and Cole (Ref. 14); other n_r determined by Arakawa *et al.* (Ref. 17).

[b] Computed with original far ultraviolet absorption spectra in Fig. 4.

[c] Computed with original far ultraviolet absorption spectra scaled up by 2.5%.

[d] Computed with original far ultraviolet absorption spectra scaled up by 5.7%.

Absorption-Index Spectrum of Solid Methane

0–500-cm^{-1} Spectral Region

The two data sets in this spectral region are those of OFMVK[7] and SF.[2] Because the data for both sets are spectral transmissions, transformation to absorption indices according to Eq. (2) will include some

Table 2. Optical Constants of Liquid Methane[a]

Frequency (cm^{-1})	n_r (111 K)	n_i (111 K)	n_r (90 K)	n_i (90 K)	Wavelength (μm)
0.0	1.274	0.000	1.293	0.000	—
140.0	1.273	1.353×10^{-3}	1.292	1.442×10^{-3}	71.43
240.0	1.272−	6.234×10^{-4}	1.291−	6.645×10^{-4}	41.67
1210.0	1.310+	1.001×10^{-2}	1.332+	1.067×10^{-2}	8.26
1230.0	1.305−	2.002×10^{-2}	1.326−	2.135×10^{-2}	8.13
1282.5	1.342+	7.499×10^{-2}	1.365+	7.994×10^{-2}	7.80
1300.0	1.258	1.600×10^{-1}	1.275	1.706×10^{-1}	7.69
1317.5	1.182−	7.249×10^{-2}	1.195−	7.728×10^{-2}	7.59
2800.0	1.284+	1.000×10^{-2}	1.303+	1.066×10^{-2}	3.57
2915.0	1.281−	2.000×10^{-2}	1.301−	2.132×10^{-2}	3.43
2965.0	1.291+	3.500×10^{-2}	1.311+	3.731×10^{-2}	3.37
3000.0	1.260	7.000×10^{-2}+	1.278	7.462×10^{-2}+	3.33
3040.0	1.227−	3.000×10^{-2}	1.243−	3.198×10^{-2}	3.29
5120.0	1.267	8.393×10^{-7}+	1.285	8.947×10^{-7}+	1.953
5175.0	1.267	1.476×10^{-6}+	1.285	1.574×10^{-6}+	1.932
8055.0	1.268	7.903×10^{-8}+	1.287	8.425×10^{-8}+	1.241
8095.0	1.268	1.573×10^{-7}+	1.287	1.677×10^{-7}+	1.235
9865.0	1.269	9.438×10^{-7}+	1.288	1.006×10^{-6}+	1.014
10 000.0	1.269	7.799×10^{-7}+	1.288	8.313×10^{-7}+	1.000
10 130.0	1.269	5.892×10^{-7}+	1.288	6.281×10^{-7}+	0.9872
10 265.0	1.269	4.651×10^{-7}+	1.288	4.958×10^{-7}+	0.9742
11 255.0	1.270	1.782×10^{-6}+	1.288	1.899×10^{-6}+	0.8885
11 530.0	1.270	3.106×10^{-7}+	1.288	3.311×10^{-7}+	0.8673
11 880.0	1.270	4.689×10^{-8}+	1.289	4.998×10^{-8}+	0.8418
12 510.0	1.270	5.725×10^{-8}+	1.289	6.103×10^{-8}+	0.7994
12 740.0	1.270	3.748×10^{-8}+	1.289	3.995×10^{-8}+	0.7849
13 700.0	1.271	9.294×10^{-8}+	1.290	9.907×10^{-8}+	0.7299
13 940.0	1.271	1.085×10^{-7}+	1.290	1.156×10^{-7}+	0.7174
14 170.0	1.271	7.862×10^{-9}+	1.290	8.381×10^{-9}+	0.7057
14 585.0	1.271	2.510×10^{-9}+	1.290	2.675×10^{-9}+	0.6856
14 935.0	1.272	4.476×10^{-9}+	1.290	4.771×10^{-9}+	0.6696
16 090.0	1.272	1.830×10^{-7}+	1.291	1.951×10^{-7}+	0.6215
16 715.0	1.273	1.095×10^{-9}+	1.292	1.167×10^{-9}+	0.5983
17 150.0	1.273	1.160×10^{-9}+	1.292	1.237×10^{-9}+	0.5831
25 000.0	1.280	0.000	1.300	0.000	0.4000
74 773.0	1.659+	1.702×10^{-1}	1.704+	1.814×10^{-1}	0.1337
83 333.0	1.455	3.128×10^{-1}+	1.486	3.336×10^{-1}+	0.1200
86 051.0	1.442−	3.024×10^{-1}	1.472−	3.225×10^{-1}	0.1162
91 991.2	1.476+	3.527×10^{-1}	1.508+	3.761×10^{-1}	0.1087
98 809.5	1.417−	4.472×10^{-1}	1.446−	4.768×10^{-1}	0.1012
100 000.0	1.420+	4.551×10^{-1}	1.448+	4.853×10^{-1}	0.1000
111 111.0	1.196	6.096×10^{-1}+	1.209	6.501×10^{-1}+	0.0900
183 333.5	0.864−	2.004×10^{-1}	0.856−	2.137×10^{-1}	0.0545
5 000 000.0	1.000	0.000	1.001	0.000	0.0020

[a]Optical constants followed by a plus or minus indicate a local maximum or minimum, respectively.

residual cell window effects that cannot be adequately accounted for because of insufficient information. Given this limitation, the resulting absorption indices are illustrated in Fig. 5. There is some difference between the two sets, a large part of which may be the result of the fact that the OFMVK data were taken at 30 K (absorption peak at 100 cm^{-1}) and the SF data were taken at 77 K (absorption peak at 160 cm^{-1}). We assume that this difference is real and use both data sets in the optical-constants analysis. At frequencies between 200 and 500 cm^{-1}, no ice data are available, so we used the corresponding liquid-methane absorption indices of ATD[3] and WLC,[4] scaled to both the OFMVK and SF data. This extrapolation is also shown in Fig. 5 for the SF data only. The absorption-index uncertainty was estimated to be 15% for values shortward of 200 cm^{-1} and 25% for those extrapolated values between 200 and 500 cm^{-1}.

500–4000-cm^{-1} Spectral Region

The three absorption-index data sets available in this spectral region are those of FS,[8] RWSP,[9] and PNOK,[11] and all are shown in Fig. 6. The numerical values of the FS absorption coefficients were supplied by Fink.[20] This data set at 52 K certainly pertains to phase I; the RWSP data set at approximately 20 K may pertain to phase II. The FS coefficients, however, were not corrected for variable interface reflection effects within the cell. Thus, in the region of strong sample absorption where the refractive index is varying, simply

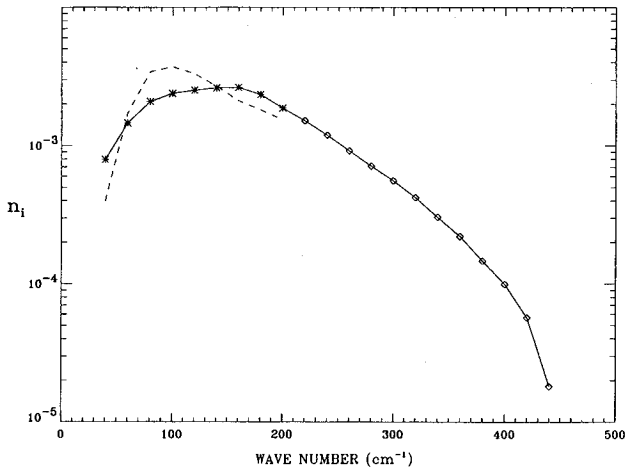

Fig. 5. Absorption-index spectra of solid methane: Dashed curve, OFMVK; asterisks, SF; diamonds, extrapolation; solid curve, best estimate.

using Eq. (2) to determine the absorption coefficient, as FS have done, will result in some error. The data of RWSP, on the other hand, were analyzed with all the cell effects taken into account, and the results are displayed as optical constants. The absorption-coefficient values of the PNOK data, supplied by Pearl,[21] are the result of an analysis similar to that of RWSP. The three absorption-index spectra show general agreement with one another in the regions of strong absorption. Some differences between the spectra can be attributed to the incomplete analysis of the FS data as described above and possibly to the different temperatures of the methane samples. At frequencies between 2300 and 3700 cm^{-1}, however, the RWSP data show a substantial absorption continuum, in contrast to the FS and PNOK data. Another such region is evident between 700 and 900 cm^{-1}. It is not clear what the nature of this absorption might be, or if it is an artifact of the analysis process. There are indications of contamination by trace constituents in the RWSP data, with at least one sharp absorption feature that probably is due to CO_2 showing up at 2340 cm^{-1}. In the FS spectrum there is also an unidentified feature at 3700 cm^{-1} that may also be the result of some contaminant. In view of the differences between the various data sets, we have selected the PNOK data in our analysis because they appear to be free of the unexplainable features that seem to plague the other two data sets, particularly that of RWSP, and also because of the rigorous analysis that the transmission data underwent to account for sample cell optical effects, unlike those of the FS data. PNOK estimated the absorption-index uncertainty to be approximately 15% in this spectral region.

4000–9000-cm^{-1} Spectral Region

The absorption indices of PNOK[11] measured at 30 K were used in this spectral region, and the results are shown in Fig. 7. The results should be quite good because substrate optical effects were accounted for in their analysis. PNOK estimated the uncertainties in these absorption indices to be approximately 20%.

Frequencies Greater than 9000 cm^{-1}

The only data in this region, those of Dressler and Schnepp,[12] start at 72 000 cm^{-1} (140 nm) and were taken at a temperature of 4.2 K. These data show that the far-ultraviolet absorption is blue shifted approximately 5 nm from that of the gaseous phase. This corresponds to an approximate 2500-cm^{-1} shift toward higher frequencies, which is considerably larger than the shifts observed throughout the rest of the spectrum. When we compare the gas and liquid phases, for example, the observed shift of the liquid-absorption peaks in the visible and the near infrared is approximately 50 cm^{-1} toward lower frequencies.[1] From the data reviewed in this paper, the observed absorption-peak shifts between the liquid and the phase I solid states are also considerably less than 50 cm^{-1}. Therefore the Dressler and Schnepp data, which correspond to solid phase III, are probably not

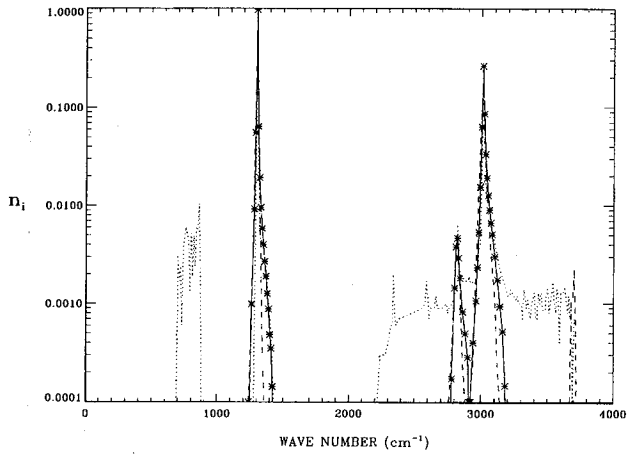

Fig. 6. Absorption-index spectra of solid methane: Dotted curve, RWSP; dashed curve, FS; asterisks, PNOK; solid curve, best estimate.

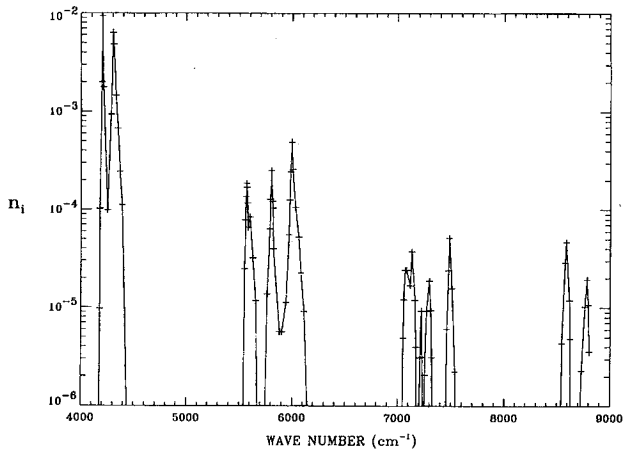

Fig. 7. Absorption-index spectra of solid methane: Crosses, PNOK; solid curve, best estimate.

indicative of the absorption characteristics of phase I. Considerable variation in the absorption spectrum between phase I and phases II or III also occurs in the far-infrared-region.[2,3] We have, therefore, assumed in our analysis that the phase I solid state for methane has an absorption spectrum shortward of 167 nm, which is more similar to the liquid or gaseous state than to the phase II or III solid state, and as such we have again used the gaseous absorption data, now scaled to the density of the phase I solid state at the melting point (see Fig. 4). At a melting-point temperature of 90 K the density is assumed to be 0.492 gm cm^{-3} (see Costantino and Daniels[13]). The estimated uncertainties in the absorption indices are the same as for liquid methane, approximately 50%.

Optical Constants of Solid Methane

In an analysis similar to that for liquid methane, the Kramers–Kronig relation, expressed by Eq. (1), was used to obtain the refractive-index spectra of phase I solid methane at the melting point (90 K) and at 30 K. Because many of the original absorption-index spectra described above were obtained at temperatures near 30 K, the n_i displayed in Figs. 4–7 were assumed to represent the absorption spectrum of methane at 30 K. We used the same temperature-dependence correction scheme as that used for liquid methane, namely, scaling the absorption spectrum by the ratio of the densities at the two temperatures, to evaluate the n_i at 90 K. Again, because of the large uncertainties in the absorption spectrum at 30 K, this correction procedure indicates only the magnitude of the temperature dependence. The Kramers–Kronig analysis with this 90 K spectrum resulted in a value for $n_r(0)$ of 1.310, smaller than the values of 1.319 and 1.320 implied from the static dielectric constants determined by Amey and Cole[14] and Costantino and Daniels,[13] respectively. By permitting the scaling of the far-ultraviolet part of the absorption spectrum to be adjusted upward by 2.9%, however, we could bring the computed $n_r(0)$ into agreement with the static dielectric constant measurements of Refs. 13 and 14.

PNOK[11] also determined refractive indices between 1200 and 4500 cm^{-1} for phase I solid methane at 30 K. Rescaling the original 30 K far-ultraviolet absorption spectrum upward by 4.0% allows us to match these refractive indices, resulting in an $n_r(0)$ at 30 K equal to 1.329. It was noted by PNOK that their refractive indices were in good agreement with those derived by RWSP.[9]

The optical constants of phase I solid methane at 90 and 30 K are listed in Table 3 for selected frequencies. The positive and negative sign convention has the same meaning as in Table 2. More complete versions of Tables 2 and 3 can be obtained from the authors.

Discussion

We have used a variety of data sources to obtain a complete spectrum of the optical constants for both liquid and phase I solid methane. Although the absorption data in certain spectral regions from multiple sources showed some significant differences, there appear to be no major problems in the relation of refractive index n_r to absorption index n_i with the Kramers–Kronig expression. More explicitly, the values of n_r computed with the Kramers–Kronig expression are in reasonably good agreement with the experimentally determined values.

There is, however, a troubling inconsistency between the value of $n_r(0)$ for liquid methane at the boiling point (111 K) as determined by Amey and Cole[14] and the values of n_r at visible wavelengths as determined by Arakawa *et al.*[16] Recall that Amey and Cole obtained a value for the static dielectric constant ε_s of 1.623 that was equivalent to $n_r(0) = 1.274$. But this value could not be fit simultaneously in the Kramers–Kronig analysis with the Arakawa *et al.* refractive-index values for any reasonable adjustments to the far-ultraviolet-region absorption coefficients. The Amey and Cole value of ε_s, however, is consistent with an essentially constant Clausius–Mossotti (CM) function,

$$\mathrm{CM} = \frac{\varepsilon_s - 1}{\varepsilon_s + 2}\frac{M}{\rho}, \tag{3}$$

which is evaluated in Table 4 for the liquid phase at 111 K (boiling point), the liquid and the solid phases at 90 K (melting point), and the solid phase at 30 K. Here M is the molecular weight, which is equal to 16.05, and ρ is the density in gm cm^{-3}. We determined the density at 30 K, 0.502 gm cm^{-3}, by extrapolating the temperature- and density-dependent empirical function for ε_s of Costantino and Daniels[13] down to 30 K and using the value for ε_s of 1.766 [$n_r(0) = 1.329$] obtained from fitting the refractive indices of PNOK[11] as described earlier. If $n_r(0)$ of liquid methane at the boiling point is assumed to be 1.282, the value that we obtained by fitting the refractive indices of Arakawa *et al.*, then ε_s is 1.644 and the value of the CM function becomes 6.69, which is considerably larger than the values of the CM function for the other temperatures given in Table 4.

For this reason $n_r(0) = 1.274$ is considered to be a more accurate value than 1.282, and therefore the former value was used in the Kramers–Kronig analysis of the 111 K absorption spectrum, the results of which are displayed in Table 2. Using this lower value for $n_r(0)$, we found that the computed n_r at visible wavelengths are approximately 0.01 lower than those determined by Arakawa *et al.* which implies that some systematic error may have entered into their measurements. The trend of the refractive indices of Arakawa *et al.* also deviates somewhat from that of the Kramers–Kronig analysis in that those indices in the blue region of the spectrum around 25 000 cm^{-1} exhibit less of an increase with frequency than expected when we consider the strong far-ultraviolet absorption upturn near 70 000 cm^{-1}.

Table 3. Optical Constants of Solid Methane[a]

Frequency (cm^{-1})	n_r (90 K)	n_i (90 K)	n_r (30 K)	n_i (30 K)	Wavelength (μm)
0.0	1.319	0.000	1.329	0.000	—
100.0	1.318	2.387×10^{-3}	1.327	3.740×10^{-3}	100.00
160.0	1.317	2.636×10^{-3}+	1.326	2.114×10^{-3}	62.50
275.0	1.316−	7.624×10^{-4}	1.326−	7.624×10^{-4}	36.36
1297.0	1.845+	5.199×10^{-1}	1.866+	5.305×10^{-1}	7.71
1300.0	1.265	9.598×10^{-1}+	1.274	9.794×10^{-1}+	7.69
1302.9	0.810−	4.585×10^{-1}	0.809−	4.679×10^{-1}	7.68
2805.0	1.321+	2.570×10^{-3}	1.331+	2.622×10^{-3}	3.57
2820.0	1.319	4.574×10^{-3}+	1.329	4.667×10^{-3}+	3.55
2830.0	1.318−	2.877×10^{-3}	1.328−	2.936×10^{-3}	3.53
3002.8	1.451+	1.107×10^{-1}	1.463+	1.130×10^{-1}	3.33
3010.0	1.339	2.564×10^{-1}+	1.349	2.617×10^{-1}+	3.32
3016.8	1.190−	1.312×10^{-1}	1.193−	1.388×10^{-1}	3.32
4200.0	1.316+	5.547×10^{-3}	1.325+	5.660×10^{-3}	2.38
4203.0	1.312	9.199×10^{-3}+	1.321	9.387×10^{-3}+	2.38
4207.5	1.306−	5.058×10^{-3}	1.316−	5.161×10^{-3}	2.38
4293.0	1.314+	3.096×10^{-3}	1.323+	3.160×10^{-3}	2.33
4303.0	1.310	6.189×10^{-3}+	1.320	6.316×10^{-3}+	2.32
4315.0	1.307−	3.453×10^{-3}	1.317−	3.523×10^{-3}	2.32
5567.0	1.311	1.807×10^{-4}+	1.321	1.844×10^{-4}+	1.796
5602.0	1.311	8.213×10^{-5}+	1.321	8.381×10^{-5}+	1.785
5802.0	1.311	2.446×10^{-4}+	1.321	2.496×10^{-4}+	1.724
5993.0	1.311	4.737×10^{-4}+	1.321	4.833×10^{-4}+	1.669
7082.0	1.312	2.368×10^{-5}+	1.322	2.416×10^{-5}+	1.412
7131.0	1.312	3.642×10^{-5}+	1.322	3.716×10^{-5}+	1.402
7220.0	1.312	9.073×10^{-6}+	1.322	9.258×10^{-6}+	1.385
7294.0	1.312	1.828×10^{-5}+	1.322	1.866×10^{-5}+	1.371
7483.0	1.312	5.023×10^{-5}+	1.322	5.126×10^{-5}+	1.336
8587.0	1.313	4.577×10^{-5}+	1.322	4.671×10^{-5}+	1.165
8784.0	1.313	1.900×10^{-5}+	1.322	1.939×10^{-5}+	1.138
10 000.0	1.313	0.000	1.323	0.000	1.000
25 000.0	1.326	0.000	1.336	0.000	0.4000
74 773.0	1.767+	1.981×10^{-1}	1.791+	2.042×10^{-1}	0.1337
83 333.0	1.530	3.632×10^{-1}+	1.546	3.744×10^{-1}+	0.1200
86 051.0	1.515−	3.518×10^{-1}	1.531−	3.627×10^{-1}	0.1162
91 991.0	1.554+	4.104×10^{-1}	1.571+	4.231×10^{-1}	0.1087
98 810.0	1.486−	5.203×10^{-1}	1.501−	5.364×10^{-1}	0.1012
101 316.0	1.491+	5.681×10^{-1}	1.506+	5.856×10^{-1}	0.0987
111 111.0	1.228	7.096×10^{-1}+	1.235	7.315×10^{-1}+	0.0900
183 334.0	0.842−	2.332×10^{-1}	0.837−	2.404×10^{-1}	0.0545
875 000.0	0.993+	2.607×10^{-3}	0.993+	2.688×10^{-3}	0.0114
5 000 000.0	0.971	0.000	0.970	0.000	0.0020

[a]Optical constants followed by a plus or minus indicate maximum or minimum, respectively.

It is possible to achieve a better fit of the measured trend, but it would require that the peak absorption near 110 000 cm^{-1} (see Fig. 4) be shifted to much higher frequencies (to approximately 150 000 cm^{-1}) and that the total absorption be substantially increased (by approximately 75%). Such a distortion of the far-ultraviolet absorption spectrum seems unwarranted.

Table 4. Clausius–Mossotti (CM) Function for Methane

T (K)	ρ (gm cm^{-3})	ε_s	CM (cm^3 mol^{-1})
111	0.424[a]	1.623[a]	6.51
90 (liquid)	0.452[b]	1.672[a]	6.50
90 (solid)	0.492[b]	1.740[a]	6.45
30	0.502[b]	1.766[c]	6.50

[a]Ref. 14.
[b]Ref. 13.
[c]See text.

Khare *et al.*[10] used the liquid-methane refractive indices of Arakara *et al.* to infer the refractive indices of solid methane by means of the Lorentz–Lorenz relationship,

$$\frac{n_s^2 - 1}{n_s^2 + 2}\frac{1}{\rho_s} = \frac{n_l^2 - 1}{n_l^2 + 2}\frac{1}{\rho_l}, \tag{4}$$

where n is the refractive index, ρ is the density, and the subscripts l and s refer to liquid and solid, respectively. This relationship is generally valid for spectral regions with negligible absorption. Khare *et al.* found that the values of n_s (ranging from 1.304 to 1.296 between 0.4 and 2.0 μm) calculated with Eq.

(4) were in good agreement with their independent determination of refractive indices (1.31 ± 0.02 in the same wavelength range and 1.302 ± 0.002 at 0.633 μm) by the use of interference-reflectance measurements of solid methane samples. However, their assumed value for ρ_s at 33 K used in Eq. (4) was 0.449 gm cm^{-3}, which is outside the accepted value range of 0.50–0.53 gm cm^{-3} (see, e.g., Costantino and Daniels,[13] Amey and Cole,[14] Manzhelii and Tolkachev[17]). If the higher density of 0.502 gm cm^{-3} is used, as assumed in this paper, then the revised refractive indices for solid methane range from 1.344 to 1.334 between 0.4 and 2.0 μm, which is considerably larger than the Khare *et al.* values derived from measurements of solid methane samples. Therefore, these results also imply that the refractive indices of Arakara *et al.* for liquid methane are systematically too large. The refractive indices displayed in Table 3 for methane at 30 K over the same spectral range fall below these revised values but above the solid sample values, which indicates general agreement but also some unresolved inconsistencies. In particular, Khare *et al.* obtained a refractive index from the solid sample of 1.302 ± 0.002 at the wavelength of 0.663 μm, whereas our analysis indicates a higher value of 1.328 ± 0.003.

An estimate of the uncertainty in the refractive indices displayed in Tables 2 and 3 was determined by the use of the absorption indices at the limit of their estimated uncertainties and the subtractive form of Eq. (1), which permits the refractive index at a frequency σ_0 to be fixed. This modified form of Eq. (1) can be written as

$$n_r(\sigma) = n_r(\sigma_0) + \frac{2}{\pi}(\sigma^2 - \sigma_0^2)P\int_0^\infty \frac{n_i(\sigma')\sigma' d\sigma'}{(\sigma'^2 - \sigma^2)(\sigma'^2 - \sigma_0^2)}. \quad (5)$$

When we set σ_0 at zero frequency, the computed n_r uncertainty estimates for both liquid and solid methane are less than 0.002 in those regions of the spectrum where absorption is at a minimum. The two strongly absorbing regions around 1300 and 3000 cm^{-1}, however, attain uncertainties at the local n_r maxima and minima of 0.022 and 0.011, respectively, for the liquid state and 0.078 and 0.020, respectively, for the solid state. For the far-ultraviolet region it is difficult to estimate the accuracy of the computed refractive indices. We originally estimated the uncertainty in the absorption coefficients to be approximately 50%. The spectrally integrated absorption, however, must be reasonably close to the true condition because of its strong effect on $n_r(0)$, which was able to be matched with only a minimum of adjustment. The actual shape of the far-ultraviolet absorption can be expected to have some variation from the values listed in Tables 2 and 3 and graphed in Fig. 4, but at most frequencies in this region it is expected that this variation is less than approximately 20%. This then implies an n_r uncertainty of less than 0.05 at any frequency higher than 60 000 cm^{-1}.

Although there is general agreement among all the various data sets and types, absorption-data deficiencies with regard to accuracy are still a problem in various spectral regions. The collision-induced absorption for both the liquid and the solid states in the far-infrared region around 200 cm^{-1} still is not well characterized, especially for the solid state at frequencies between 200 and 500 cm^{-1}. The liquid state is characterized by only the measurements of Pinkley *et al.*[5] at the fundamental bands near 1300 and 3000 cm^{-1}, and these measurements contain relatively prominent background absorptions near the absorption peaks. Confirmation of these features would be desirable because the solid-state measurements of PNOK[11] in these same spectral regions do not show such features. The seemingly high values for the refractive indices in the visible and the near infrared of Arakawa *et al.*[16] should also be confirmed with additional measurements. Finally, any absorption data in the far ultraviolet for either the liquid or the phase I solid state would be extremely useful for validating the assumption of gaseous absorption similarity that was used in our analyses.

Application

These results have direct application to the study of atmospheres in the outer solar system. Two brief examples follow. In the first example the influence of liquid-methane clouds in the atmosphere of Titan, Saturn's largest satellite, has been modeled following the properties suggested by Toon *et al.*[22] Evidence for such clouds is quite indirect and follows only from the expectation that the amount of methane gas in the lower troposphere near Titan's surface is large enough that condensation takes place at higher and colder latitudes. The far-infrared spectrum of Titan is shown in Fig. 8, which illustrates the influence of the 100-μm droplet cloud and the submicrometer haze model preferred by Toon *et al.*[22] and is con-

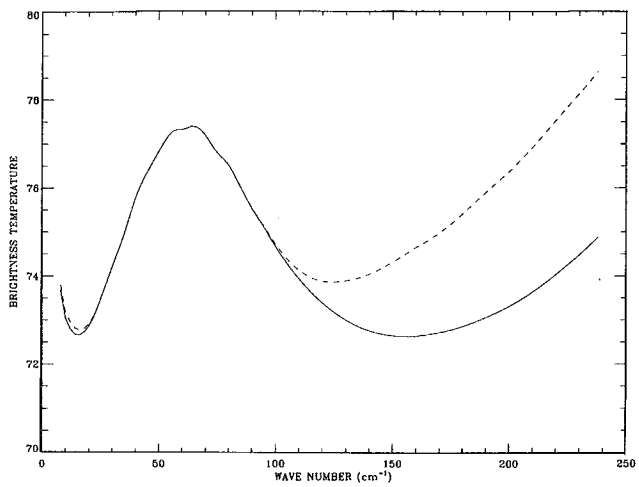

Fig. 8. Model far-IR spectra of Titan for an emission angle near 0°: Dashed curve, clear atmosphere; solid curve, atmosphere with a haze and a CH_4 condensate cloud of 100-μm droplets.

strained by Voyager infrared spectrometer data for wave numbers of 200 cm^{-1} and greater. The 60-cm^{-1} emission feature corresponds to the location of maximum N_2–N_2 collision-induced gaseous absorption. The emission feature is centered on a broad absorption region and represents thermal emission from a region where temperature is increasing with altitude (and brightness is increasing with optical thickness). Although both the haze and the methane droplet cloud influence Titan's spectrum above 60 cm^{-1} quite strongly, their influence on spectral regions below 60 cm^{-1} is negligible, even for 100-μm liquid methane droplets. Thus the spectral region shortward of 60 cm^{-1} is useful for sounding temperatures in Titan's lower atmosphere up through a level just above the temperature minimum with little confusion from known or suspected clouds or hazes.

In the second example solid methane crystals are expected to form in Neptune's troposphere near the 1.5-bar level from a large reservoir of gaseous methane in the deep atmosphere, where the methane mixing ratio is of the order of 1–2%. A comparison by Conrath *et al.*[23] of Voyager infrared and radio occultation measurements indicates that this cloud is optically significant. Three spectra are shown in Fig. 9, which simulates the conditions by which the Conrath *et al.* model spectra were computed. For the purpose of this illustration we constrained all spectra to the same brightness temperature at 200 cm^{-1}. Cloud bottoms were placed near the expected methane condensation pressure of 1.5 bars, and cloud tops were placed near the temperature minimum at 0.2 bars; the cloud-particle scale height is 0.15 times the pressure scale height. Figure 9 shows that observations of the spectrum shortward of the Voyager infrared spectrometer limit of 200 cm^{-1}, as might be obtained by the European Space Agency's Infrared Space Observatory Long Wavelength Spectrometer instrument, will distinguish between 3- and 30- or 0.3-μm but not between 30- and 0.3-μm particles. This is also true of the faint continuum near 1000 cm^{-1}, which might be detected between many stratospheric emission lines in this region (not shown in Fig. 9).

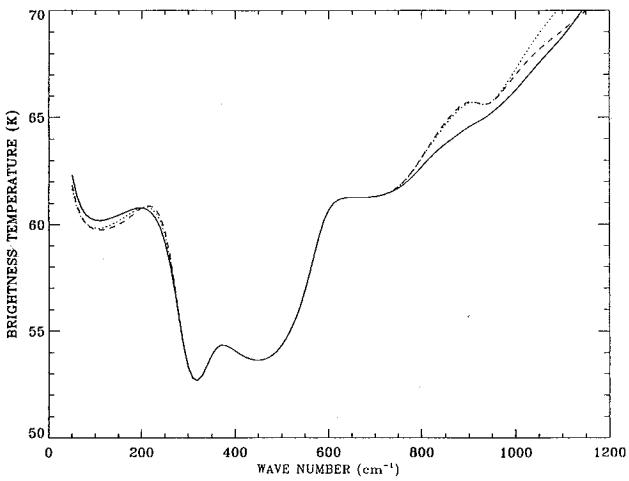

Fig. 9. Model IR spectra of Neptune with only continuum components considered. The number density of particles in a solid CH_4 cloud is adjusted in each model to obtain the same brightness temperature at 200 cm^{-1}. Dotted curve, cloud with 0.3-μm particles; solid curve, cloud with 3-μm particles; dashed curve, cloud with 30-μm particles.

Conclusion

Data on the optical properties of liquid methane and phase I solid methane, which we obtained by performing a literature search, were collectively analyzed with the Kramers–Kronig relation to determine the spectral optical constants from 0 to 500 000 cm^{-1}. Much of the data consisted of spectral transmission measurements that then were converted to absorption coefficients. In these cases corrections for sample cell multiple reflection effects were ignored, mainly because of incomplete information concerning the sample cell and also the quality of the data. For both liquid and phase I solid methane no data could be found on the strong far-ultraviolet absorption at frequencies beyond 60 000 cm^{-1}, and so the gaseous absorption spectrum in this frequency region was used as a substitute and scaled with the appropriate density ratios. Measured static dielectric constants and refractive indices in limited spectral ranges were used as constraints in the Kramers–Kronig analysis. Further improvements in the accuracy of the optical constants for both the liquid and the phase I solid states of methane will require additional measurements, particularly in the far-ultraviolet portion of the spectrum. However, the current status of the optical constants as reviewed in this paper is sufficiently to be useful in the study of the bodies of the outer solar system.

We thank J. Pearl, U. Fink, and B. Khare for tabular forms of their data and J. Pearl for many helpful comments. This research was carried out at the Jet Propulsion Laboratory, California Institute of Technology, under contract with the National Aeronautics and Space Administration.

References

1. C. K. N. Patel, E. T. Nelson, and R. J. Kerl, "Opto-acoustic study of weak optical absorption of liquid methane," Nature (London) **286,** 368–370 (1980).
2. R. Savoie and R. P. Fournier, "Far-infrared spectra of condensed methane and methane-d4," Chem. Phys. Lett. **7,** 1–3 (1970).
3. H.-J. Arning, K. Tibulski, and Th. Dorfmuller, "Collision-induced spectra of simple liquids," Ber. Bunsenges. Phys. Chem. **85,** 1068–1071 (1981).
4. S. Weiss, G. E. Leroi, and R. H. Cole, "Pressure-induced infrared spectrum of methane," J. Chem. Phys. **50,** 2267–2268 (1969).
5. L. W. Pinkley, P. P. Sethna, and D. Williams, "Optical constants of liquid methane in the infrared," J. Opt. Soc. Am. **68,** 186–189 (1978).
6. K. R. Ramaprasad, J. Caldwell, and D. S. McClure, "The vibrational overtone spectrum of liquid methane in the visible and near infrared: applications to planetary studies," Icarus **35,** 400–409 (1978).

7. J. Obriot, F. Fondere, Ph. Marteau, H. Vu, and K. Kobashi, "Far-infrared spectra of solid CH_4 under high pressure," Chem. Phys. Lett. **60,** 90–94 (1978).
8. U. Fink and G. T. Sill, "The infrared spectral properties of frozen volatiles," in *Comets,* L. L. Wilkening, ed. (U. Arizona Press, Tucson, Ariz., 1982), pp. 164–202.
9. J. A. Roux, B. E. Wood, A. M. Smith, and R. R. Plyler, "Infrared optical properties of thin CO, NO, CH_4, HCl, N_2O, O_2, N_2, Ar, and air cryofilms," Arnold Engineering Development Center Tech. Rep. AEDC-TR-79-81 (Arnold Engineering Development Center, Arnold Air Force Station, Tennessee 1979), pp. 71–74.
10. B. N. Khare, W. R. Thompson, C. Sagan, E. T. Arakawa, C. Bruel, J. P. Judish, R. K. Khanna, and J. B. Pollack, "Optical constants of solid methane," in *First International Conference on Laboratory Research for Planetary Atmospheres,* K. Fox, J. E. Allen, and D. T. Quillan, eds. (NASA, Greenbelt, Md., 1989), pp. 327–333.
11. J. Pearl, N. Ngoh, M. Ospina, and R. Khanna, "Optical constants of solid methane and ethane from 10,000 to 450 cm^{-1}," J. Geophys. Res. **96,** 17477–17482 (1991).
12. K. Dressler and O. Schnepp, "Absorption spectra of solid methane, ammonia, and ice in the vacuum ultraviolet," J. Chem. Phys. **33,** 270–274 (1960).
13. M. S. Costantino and W. B. Daniels, "Dielectric constant of compressed solid methane at low temperature," J. Chem. Phys. **62,** 764–770 (1975).
14. R. L. Amey and R. H. Cole, "Dielectric constants of liquefied noble gases and methane," J. Chem. Phys. **40,** 146–148 (1964).
15. J. V. Martonchik, G. S. Orton, and J. F. Appleby, "Optical constants of NH_3 ice from the far infrared to the near ultraviolet," Appl. Opt. **23,** 541–547 (1984).
16. E. T. Arakawa, P. D. Clapp, T. A. Calcott, B. N. Khare, and C. Sagan, "Refractive indices of liquid methane and ethane," Bull. Am. Phys. Soc. **31,** 700 (1986).
17. V. G. Manzhelii and A. M. Tolkachev, "Densities of ammonia and methane in the solid state," Sov. Phys. Solid State **5,** 2506–2510 (1964).
18. R. D. Hudson, "Critical review of ultraviolet photoabsorption cross sections for molecules of astrophysical and aeronomic interest," Rev. Geophys. Space Phys. **9,** 305–406 (1971).
19. G. H. Mount, E. S. Warden, and H. W. Moos, "Photoabsorption cross sections of methane from 1400 to 1850 Å," Astrophys. J. **214,** 47–49 (1977).
20. U. Fink, Lunar and Planetary Laboratory, University of Arizona, Tucson, Ariz. 85721 (personal communication, 3 April 1980).
21. J. Pearl, NASA Goddard Space Flight Center, Greenbelt, Md. 20771 (personal communication, 19 April 1991).
22. O. B. Toon, C. P. McKay, R. Courtin, and T. P. Ackerman, "Methane rain on Titan," Icarus **75,** 255–284 (1988).
23. B. J. Conrath, D. Gautier, G. F. Lindal, R. E. Samuelson, and W. A. Shaffer, "The helium abundance of Neptune from Voyager measurements," J. Geophys. Res. **96,** 18907–18919 (1991).